Full Paper

Propellants, Explosives, Pyrotechnics

DOI: 10.1002/prep.201400180

Fragment Velocity Distribution of Cylindrical Rings Under Eccentric Point Initiation

Guangyan Huang,[a] Wei Li,[a] and Shunshan Feng*[a]

Abstract: A design mode, in which a casing is filled with a charge initiated off-centre (eccentric point initiation), is common in the field of explosion and structural protection. The fragment velocity distribution along the circumference of the casing is distinctly non-uniform due to the difference in blast loading around the circumference of the casing. To quantify the fragment velocity distribution, two kinds of cylindrical rings with different structural parameters were adopted. Static explosive experiments with three eccentric coefficients (0, 0.5, 1.0) were conducted with pulsed X-ray diagnostics. Using coefficients derived from experimental data and calculating the effects of both the eccentricity of initiation and angle around the circumference, an angle-dependent ratio β_θ of charge mass to casing mass has been derived as a mean to modify the fragment velocity formula of Gurney for this application. The derived formula was shown to correctly predict the fragment velocity distribution around the circumference of the cylindrical ring. The calculated velocity distributions show good agreement with the experimental results.

Keywords: Fragment velocity · Gurney · Explosive load · Eccentric point initiation · Cylindrical ring

1 Introduction

Most axially symmetrical casings filled with charge are given axial initiation at one end. The fragment velocity and angles around the circumference of any section across the casing axis are uniform and lead to an evenly-distributed kinetic energy field of fragments around the axial of the casing. However, in some applications of explosive munitions [1,2], eccentric initiation is adopted instead of axial initiation. Taking a section of cylindrical casing (regarded as a ring) for discussion, the initiation point will in this case be off the center of the circle. Around the circumference, the ring is under an axially asymmetric energetic loading, generated by the eccentric initiation, which causes that the impulse exerted on the ring is asymmetrically distributed. Furthermore, the fragment velocity and the kinetic energy around the circumference of the ring are variable. Relevant explosion research is therefore directed to obtain the property of fragments velocity distribution around the circumference of cylindrical ring under eccentric initiation.

The investigation of the fragment velocity of cylindrical casing under axial initiation has been studied for decades. There exist many formulae to calculate the fragment velocity of cylindrical casing under axial initiation, such as the typical Gurney formulae [3] and the corrected Gurney formulae [4–7]. However, it is more difficult and complex to predict the fragments velocity distribution under eccentric initiation. Waggener described the asymmetrically initiated warheads and the mechanism on increasing the velocities of the warhead fragments in the target direction, in addition, he estimated velocities from the warhead by adding an additional coefficient 1.25 in Gurney's formula which takes the enhanced velocity in the target direction into account [8,9]. Hennequin obtained the enhanced coefficients on fragments velocity at the target direction by conducting the experiments where cylindrical casings with different weight ratios of the charge to the casing were initiated at an eccentric point [10]. Huang investigated the radial velocities for a double line initiation at different distance from the initiation points to the fragment layers [11]. Held used a modified form of Huang's formula [11] to calculate the velocities for single eccentric line initiation warheads. The prediction of Held's formulae gave a good agreement with the experimental data in target direction, while discrepancies in other directions occurred. Wang [12] proposed a formula to predict the radial distribution of the fragment velocities of the velocity enhanced warhead by using a correctional function. His formula calculates the velocity gains with azimuth angle and gave an accurate prediction comparable with experiment data.

Due to various eccentric initiation warheads and too many factors involved into the process of eccentric initiation, for the purpose of establishing a general calculating model, warheads with a thickness of casing and diameter of charge that vary in a linear fashion are treated as re-

[a] *G. Huang, W. Li, S. Feng*
State Key Laboratory of Explosion Science and Technology, Beijing Institute of Technology, Beijing 100081, P. R. China
**e-mail: ssfeng@bit.edu.cn*

search objects in this paper. Pulsed X-rays were used to provide velocity diagnostics on the experimental tests. However, it was impossible to obtain the fragment velocity around azimuth direction in every section of a warhead due to the sight obstruction of fragments at other axial sections. For an axisymmetric warhead, it can be treated as the combination of many infinitesimal rings with the same axial line. Hence, a single ring is treated as the model to be investigated by experiments.

2 Experimental Section

2.1 Methods

The cylindrical ring filled with charge was adopted as the typical experimental model in Figure 1. The radius and mass of the charge are r and m. The mass of cylindrical ring is M. $\beta = m/M$ is the mass ratio of the charge to cylindrical ring. e_p is the distance from the eccentric initiation point to the axis of cylindrical ring. e_p/r is defined as the eccentric coefficient. θ is the azimuth angle, which is represented by the angle between OP_θ and OO_p. θ/π is defined as the azimuth angle coefficient. ϕ_θ is the scattering angle, which is represented by the angle between O_pP_θ and OO_p. v_θ is the fragment velocity at the azimuth angle θ. This fragment velocity v_θ can be expressed as a function of the two independent variables, e_p/r and θ/π: $v_\theta = f(e_p/r, \theta/\pi)$.

A 300 kV pulsed X-ray with two parallel X-ray tubes was used in the test, as shown in Figure 2. X-ray 0 took a static photograph of specimen (the cylindrical ring filled with charge) at time t_0. X-rays 1 and 2 took two photographs at different times t_1 and t_2 in sequence. The pictures were compiled in one photograph, as shown in Figure 3.

The fragment velocities can be calculated based on the interval time $\Delta t = t_2 - t_1$ and the corresponding displacement Δx in every azimuth angle. Due to the distance L_1 from X-ray tubes to specimen and the distance L_2 from specimen to the negative plate, an amplification coefficient μ, which is the size ratio of the image in photo to the real object, exists. To obtain the displacement Δx in every azimuth angle between the interval time Δt, the fragment profile at time t_1 should be moved the distance ΔL, which is caused by the distance between two parallel X-ray tubes

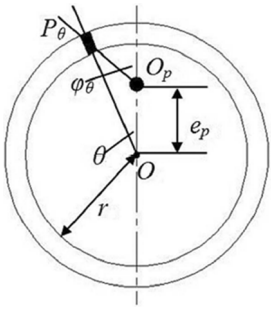

Figure 1. Typical model of the cylindrical ring filled with charge.

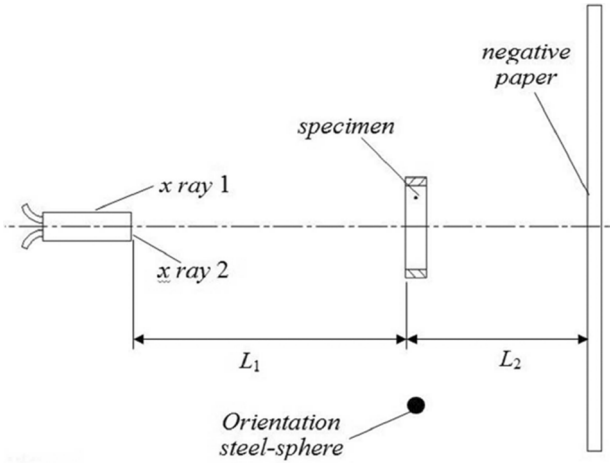

Figure 2. Schematic view of test set-up.

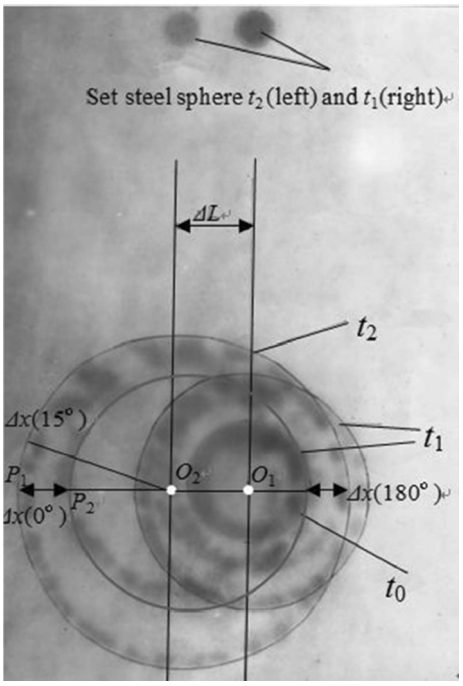

Figure 3. Schematic of the measurement method.

in order to coincide the circle center of specimen O_1 at time t_1 with O_2 at time t_2, as shown in Figure 3. The off-set distance ΔL was obtained from the image of a fiducial steel sphere. The ray from O_2 intersects with the moved fragments profile in P_1 and the fragments profile at time t_2 in P_2. Hence, Δx is the distance P_1 P_2 and the average fragment velocity is:

$$v(\theta) = \frac{\Delta x}{\Delta t} \quad (1)$$

Table 1. Two kinds of specimens with different structural parameters.

Specimen	No.	Length of ring L [mm]	Diameter of charge d [mm]	Thickness of ring δ [mm]	Mass ratio of charge to ring β	Eccentric coefficient e_{px}/r
1#	1–1	13.23	44.07	2.51	0.9615	0
	1–2					0.5
	1–3					1
2#	2–1	15.78	53.69	3.04	0.9309	0
	2–2					0.5
	2–3					1

The points P_1 and P_2 are changing with the angle θ of the ray from point O_2 (the azimuth angle).

Firstly, two kinds of specimens with different structural parameters were used for the cylindrical rings with charge, which are listed in Table 1. AISI1045 steel was adopted in the experiments as the material of metal casing. The explosive filled in the casing was TNT50/RDX50. The densities of AISI1045 and TNT50/RDX50 are 7.85 g cm^{-3} and 1.68 g cm^{-3}. The eccentric coefficients are selected as 0, 0.5 and 1.0 for these two kinds of specimen. For every eccentric coefficient, three tests were conducted and the average values treated as the fragment velocities.

2.2 Experimental Results

According to the measurement methods mentioned above, the enhancement of the fragment velocity with varying azimuth angle of the two kinds of specimens is shown in Figure 4. The fragments velocity enhancement coefficient is defined as the ratio of the fragments velocity under eccentric initiation to that under axial initiation.

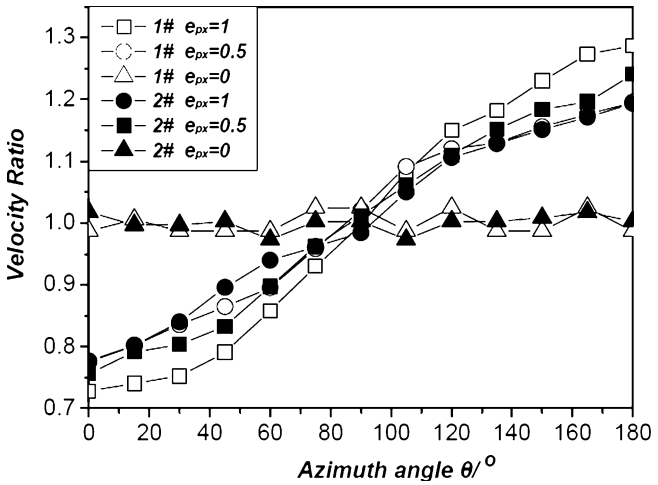

Figure 4. Change of the fragment velocity enhanced coefficient with azimuth angle of specimens 1# and 2#.

In Figure 4, it can be seen that there is a greater change of the fragments velocity enhancement coefficient with azimuth angle with the 1# specimen compared to the 2# specimen. The 1# specimen has a smaller enhancement coefficient in the azimuth angle region 0–90°and a bigger enhancement coefficient in 90–180° than the 2# specimen. Furthermore, it shows that there is little difference between the fragments velocity enhancement coefficients of 1# and 2# under the eccentric initiation $e_p = 0.5$, but a larger difference under the eccentric initiation $e_p = 1$. This can be explained as follows: While the length of 2# specimen is almost equal to that of 1# specimen, the diameter of the 2# specimen is 21.8% greater than that of 1#, which allows a greater influence of the rarefaction wave generated from the ends of charge [13]. Hence, the influence of eccentric initiation will be weakened and the fragments velocity enhancement coefficient of 2# will be closer to 1 than that of 1#. For the eccentric initiation coefficient 0.5, the difference of enhancement coefficient between specimens 1# and 2# is very small, due both to the weaker eccentric initiation effect and to the influence of the rarefaction wave. Hence, the enhanced effect of 2# is more close to axial initiation with respect to 1#.

3 Calculated Model for the Distribution of the Fragment Velocity Along the Azimuth

To simplify the calculational model, an assumption was made that the fragments velocity along the azimuth direction v_θ is just a function of the eccentric initiation coefficient e_p/r and azimuth angle coefficient θ/π. In addition, it was assumed that the scattering angle of fragments would be the same as the normal direction of cylindrical ring. Hence, based on the fragments velocity calculating formulae of axisymmetric casing filled with charge under axial initiation, v_θ can be corrected and expressed as: [14]:

$$\nu(\theta) = \sqrt{2E\beta(\theta)/[1 + 0.5\beta(\theta)]} \tag{2}$$

where, $\sqrt{2E}$ is Gurney constant of the explosive, $\beta_\theta = f(e_p/r, \theta/\pi)$, β_θ is the equivalent mass ratio of charge to cylindrical ring at the azimuth angle θ and β is the actual mass ratio of charge to cylindrical ring under axial initiation.

From Equation (2), it can be seen that the calculation of v_θ is transformed into that of β_θ. v_0 is defined as the fragment velocity at $\theta = 0$ and there must be a β_0 equivalent to β at $\theta = 0$. According to experimental results, the fragments velocity decrease with increasing e_p/r in the azimuth angle region of 0~90°. Hence, β_0 is an inverse function of e_p/r. If $f_1(e_p/r) = \beta_0/\beta$, then $f_1(e_p/r)$ will be equal to 1 at $e_p/r = 0$ and to minimum value at $e_p/r = 1$. $f_1(e_p/r)$ can be constructed as:

$$f_1(e_p/r) = 1 - a_1(e_p/r)^{a_2} \tag{3}$$

where, a_1, a_2 are the constants obtained by regressing the experimental data. Based on these, Equation (3) can be expressed as:

$$f_1(e_p/r) = \beta_0/\beta = \begin{cases} 1 - 0.47(2e_p/r)^{0.75} & 0 \le e_p/r \le 0.5 \\ 1 - 0.53(2e_p/r)^{0.17} & 0.5 \le e_p/r \le 1 \end{cases} \tag{4}$$

From the experimental results, v_θ is increasing with increase of θ. It can concluded that β_θ is increasing with the increasing of θ. The distance $|P_\theta O_1|$ from point P_θ to point O_1 is a function of e_p/r and θ, as shown in Figure 1.

λ is defined as the distance coefficient $|P_\theta O_1|/r$ and can be expressed as:

$$\lambda = [4(e_p/r)\sin^2(\theta/2) + (1 - e_p/r)^2]^{0.5} \tag{5}$$

In the same way, $f_2(e_p/r, \theta/\pi)$ is defined as β_θ/β_0 and can be constructed as:

$$f_2(e_p/r, \theta/\pi) = \beta_\theta/\beta_0 = 1 + a_3(\theta/\pi)(e_p/r)^{a_4} e^{a_5\lambda} \tag{6}$$

where a_3, a_4 and a_5 are constants obtained by regressing the experimental data. Equation (6) can expressed as:

$$f_2(e_p/r, \theta/\pi) = \begin{cases} 1 + 2(\theta/\pi)(e_p/r)e^{K_1\lambda} & \begin{matrix} 0 \le \theta \le \pi \\ 0 \le e_p/r \le 0.5 \end{matrix} \\ 1 + (\theta/\pi)(e_p/r)^{0.1} e^{K_2\lambda} & \begin{matrix} 0 \le \theta \le \pi \\ 0.5 \le e_p/r \le 1 \end{matrix} \end{cases} \tag{7}$$

where, K_1 and K_2 are 0.6 and 0.74. Combining Equation (4) and (7), the function of β_θ can be expressed as:

$$\beta_\theta/\beta = f(e_p/r, \theta/\pi) = \begin{cases} [1 - 0.47(2e_p/r)^{0.75}][1 + 2(\theta/\pi)(e_p/r)e^{K_1\lambda}] & \begin{matrix} 0 \le \theta \le \pi \\ 0 \le e_p/r \le 0.5 \end{matrix} \\ [1 - 0.53(2e_p/r)^{0.17}][1 + (\theta/\pi)(e_p/r)^{0.1} e^{K_2\lambda}] & \begin{matrix} 0 \le \theta \le \pi \\ 0.5 \le e_p/r \le 1 \end{matrix} \end{cases} \tag{8}$$

An expression for v_θ can now be obtained by substituting Equation (5) and (8) into Equation (2).

4 Comparison of Calculated and Experimental Results

4.1 Azimuthal Distribution of the Fragment Velocity

To demonstrate the applicability of the above formulae, a comparison of calculated and experimental results is shown in Figure 5 and Figure 6.

From Figure 5, for specimen 1#, and for $e_p/r = 0.5$, it can be seen that a good agreement between calculated results and experimental data exists, except a slight deviation in the azimuth angle region of 110–130°. Here the calculated results show that the enhancement coefficient of the frag-

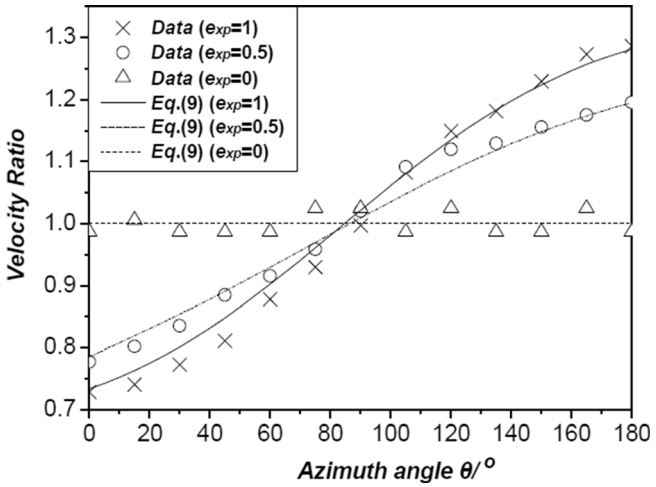

Figure 5. Comparison of calculated and experimental fragment velocity enhanced coefficients changing with azimuth angle 1#.

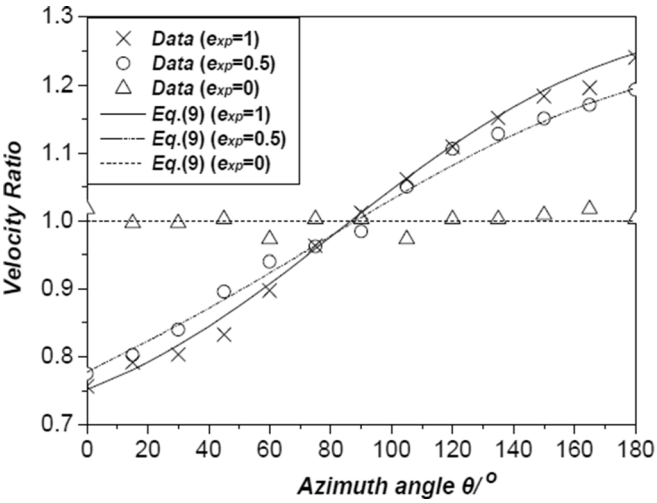

Figure 6. Comparison of calculated and experimental fragment velocity enhanced coefficients changing with azimuth angle 2#.

ment velocity increases smoothly with increasing azimuth angle in this region, while the experimental data maintain near-constant higher values. For $e_p/r=1$, good agreement between the calculated results and the experimental data exists, except a slight deviation in the azimuth angle region of 30–50°.

From Figure 5 and Figure 6, the fragment velocity enhancement coefficient for specimen 2# is closer to 1.0 than that of 1#, which indicates that the bigger the diameter of charge, the longer the time of detonation and expansion and the more uniform the phase of detonation product. Furthermore, the difference between the calculated curves and the experimental data of 2# is less than that of 1#.

4.2 Azimuthal Distribution of the Kinetic Energy of the Fragments

E_θ is defined as the sum of the kinetic energies of the fragments in the azimuth angle range from 0 to θ, E_π is defined as the sum of the kinetic energies of the fragments in the azimuth angle range from 0 to π. The ratio of E_θ to E_π can be expressed as:

$$\frac{E_\theta}{E_\pi}=\frac{\int_0^\theta v_\theta^2 d\theta}{\int_0^\pi v_\theta^2 d\theta}=\frac{\int_0^\theta \left(\frac{v_\theta}{v}\right)^2 d\theta}{\int_0^\pi \left(\frac{v_\theta}{v}\right)^2 d\theta}=\frac{T_\theta}{T_\pi} \tag{9}$$

where, v is the fragments velocity of cylindrical ring under axial initiation. T_θ is defined as:

$$T_\theta=\int_0^\theta \left(\frac{v_\theta}{v}\right)^2 d\theta \tag{10}$$

By substituting Equations (2), (5) and (8) into Equation (10), T_θ can be obtained as:

$$T_\theta=\int_0^\theta \left(\frac{v_\theta}{v}\right)^2 d\theta=\int_0^\theta \frac{\beta_\theta/(1+0.5\beta_\theta)}{\beta/(1+0.5\beta)}d\theta=\frac{1}{\beta/(1+0.5\beta)}\int_0^\theta \frac{a+b\theta}{1+0.5(a+b\theta)}d\theta \tag{11}$$

where, a and b can be obtained from Equations (5) and (8) by:

$$a=\begin{cases}1-0.47(2e_p/r)^{0.75} & 0\le e_p/r\le 0.5\\ 1-0.53(2e_p/r)^{0.17} & 0.5\le e_p/r\le 1\end{cases} \tag{12}$$

and

$$b=\begin{cases}\frac{2}{\pi}[1-0.47(2e_p/r)^{0.75}](e_p/r)e^{K_1\lambda} & 0\le e_p/r\le 0.5\\ \frac{1}{\pi}[1-0.53(2e_p/r)^{0.17}](e_p/r)^{0.1}e^{K_2\lambda} & 0.5\le e_p/r\le 1\end{cases} \tag{13}$$

By substituting Equation (11) into Equation (9), the azimuth distribution of the kinetic energies of the fragments can be obtained. The azimuth distributions of specimens 1# and 2# are shown in Figure 7 and Figure 8. In addition, the experimental points for kinetic energy were derived from the experimental velocity data.

As shown in Figure 7 and Figure 8, there is a good agreement between calculated curves and experimental data.

It can be seen that the fraction of the total fragment kinetic energy over azimuth angle from 0 to 90° is 0.5 under axial initiation. This is because the shock wave and detonation product exert on the cylindrical ring, uniformly. However, for $e_p/r=0.5$, to find the mid-point in the kinetic energy distribution, the azimuth angle range has to be from 0 to 106° and from 0 to 107° for 1# and 2#, respectively. For $e_p/r=1$, the required azimuth angle ranges are from 0 to 112° and from 0 to 113° for 1 and 2#, respectively. This indicates that the detonation energy of charge is inhomogeneously distributed around the azimuth direction of cylindrical ring. With increasing eccentric coefficient e_p/r,

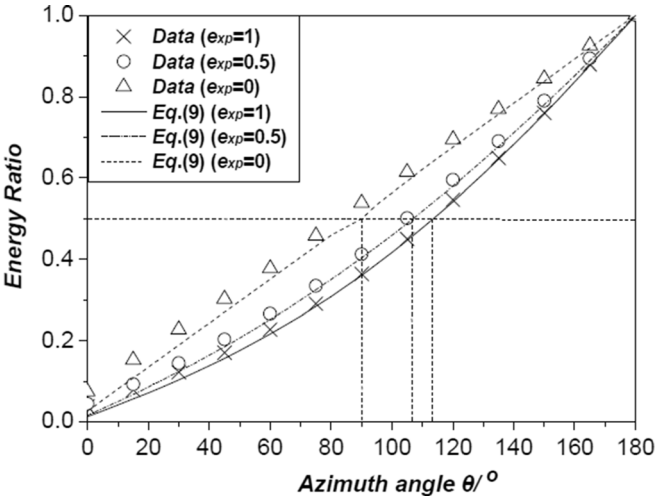

Figure 7. Azimuth distribution of the fragments with energy ratio 1#.

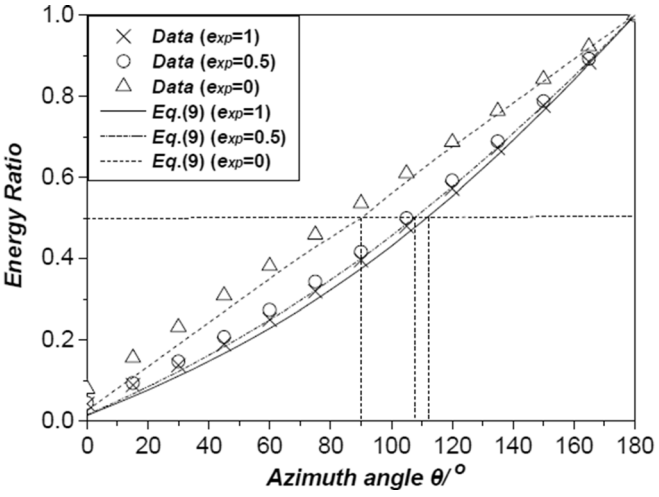

Figure 8. Azimuth distribution of the fragments with energy ratio 2#.

the azimuth angle range near the initiation point with 50% energy ratio is increasing, while that far from the initiation point is decreasing. Hence, the part of ring far from the initiation point receives more detonation energy and the fragment velocity at 180° is as its maximum value. The energy ratio curves are concave upward under eccentric initiation, i.e. there is pronounced enhancement of the fragments velocity at the part of ring farthest from the initiation point, as shown in Figure 7 and Figure 8.

In addition, it can be seen from Figure 7 and Figure 8 that the energy ratio curve of $e_p/r = 0.5$ runs below that of $e_p/r = 0$ and above that of $e_p/r = 1$. The change of e_p/r from 0 to 0.5 is same as that from 0.5 to 1, but the difference between energy ratio curves from $e_p/r = 0.5$ to 1 is much less than that from $e_p/r = 0$ to 0.5. This indicates that the effect of gradually increasing eccentricity of initiation in enhancing velocity at points far from the initiation point diminishes as e_p/r increases.

5 Conclusion

Linked to an experimental investigation, the new formulae for the azimuth distribution v_θ of the fragment velocities of cylindrical rings under eccentric initiation are proposed. Two kinds of typical specimens have been tested under eccentric initiation ($e_p/r = 0$, 0.5 and 1) and the experimental data of the azimuth distributions of the fragments velocities were recorded by means of 300 kV pulsed X-ray sets with two parallel X-ray tubes.

Based on a modification of Gurney's formula, new formulae for v_θ the fragment velocity as a function of azimuth angle θ and eccentric initiation coefficient e_p/r are proposed. Firstly, the calculation of v_θ was translated into that of an equivalent mass ratio β_θ of charge to cylindrical ring at every azimuth angle θ. Secondly, the mass ratio β_0 was obtained by considering the effect of eccentric initiation coefficient e_p/r on the mass ratio β at azimuth angle 0; Finally, the equivalent mass ratio β_θ was obtained by considering the effect of azimuth angle θ on the relationship between β_θ and β_0. Above all, the formulae of v_θ can be obtained. Comparison with the experimental data, the calculated results of the formulae of v_θ has a good agreement, which indicates that the formulae of v_θ can predict the fragments velocity azimuth distribution of cylindrical ring under eccentric initiation.

In addition, the calculated fragments kinetic energy azimuth distribution has been compared with experimental data. It could be seen that the detonation energy of charge was in homogeneously distributed around the azimuth direction of cylindrical ring; the parts of the ring far from the initiation point receiving more detonation energy with the increase of eccentric initiation coefficient. Also, the effective enhancement on the part farthest from the initiation point did not increase in proportion to increase in e_p/r.

Acknowledgments

This work was sponsored by the National Natural Science Foundation of China under Grant Nos. 11102023 and 11172071, and the Foundation of State Key Laboratory of Explosion Science and Technology of China under Grant No. YBKT15-02. The authors wish to express their appreciation to personnel at Intensive Loading Effects Research Group of State Key Laboratory of Explosion Science and Technology, where the experimental data reported on this paper were collected.

References

[1] S. S. Feng, *New Technology to Enhance Damage Efficiency of Missile Fragmentation Warhead*, Internal Report GFYJ 93, Beijing Institute of Technology, Beijing, P. R. China, **1994**.
[2] R. M. Lloyd, *Physics of Direct Hit and Near Miss Warhead Technology, Progress in Astronautics and Aeronautics*, Volume 194, American Institute of Aeronautics and Astronautics, Reston, **2001**.
[3] R. W. Gurney, *The Initial Velocities of Fragments from Bombs, Shells and Grenades*, BRL Report No 405, Ballistic Research Laboratory, Aberdeen Proving Ground, MD, USA, **1943**.
[4] G. Randers-Pehrson, An Improved Equation for Calculating Fragment Projection Angles, *2nd International Symposium on Ballistics*, Daytona Beach, FL, USA, **1976**.
[5] Y. J. Charron, *Estimation of Velocity Distribution of Fragmenting Warheads Using A Modified Gurney Method*, AD-A074759, Air Force Institute of Technology, Wright-Patterson AFB, OH, Canada, **1979**.
[6] E. Hennequin, Influence of the Edge Effects on the Initial Velocity of Fragments from a Warhead, *9th International Symposium on Ballistics*, Shrivenham, UK, **1986**.
[7] S. S. Feng, B. G. Cui, J. W. Jiang, An Experimental Investigation for the Axial Distribution of Initial Velocity of Shells, *Acta Armamentarii*, **1987**.
[8] S. Waggener, Relative Performance of Anti-Air Missile Warheads, *19th International Symposium on Ballistics*, Interlaken, Switzerland, May 7–11, **2001**.
[9] S. Waggener, The Evolution of Air Target Warheads, *23rd International Symposium of Ballistics*, Tarragona, Spain, April 16–20, **2007**.
[10] E. Hennequin, L. Claude, J. Diet, Evaluation of Fragment Velocity of Aimable Warheads, *17th International Symposium of Ballistics*, Midrand, South Africa, March 23–27, **1998**.
[11] M. Held, Velocity Enhanced Warheads, *J. Explos. Propellants* **2001**, *17*, 1–12.
[12] M. F. Wang, F. Y. Lu, A Formula for Calculating the Velocities of Fragments from Velocity Enhanced Warhead, *Propellants Explos. Pyrotech.* **2013**, *38*, 232–237.
[13] D. Grady, *Fragmentation of Rings and Shells, The Legacy of N. F. Mott*, Springer, Berlin, Heidelberg, **2010**.
[14] S. S. Feng, J. W. Jiang, S. L. He, S. L. Zhou, On the Pattern of Radial Distribution Pattern of Initial Velocities of Fragments Under Asymmetrical Initiation, *Acta Armamentarii* **1993**, *Supplement*, 12–16.

Received: July 28, 2014
Revised: October 7, 2014
Published online: December 2, 2014

